An Efficient Parameterization for Surface Shortwave 3D Radiative Effects in Large-Eddy Simulations of Shallow Cumulus Clouds

Mirjam Tijhuis[1], Bart J. H. van Stratum[1], Menno A. Veerman[1], and Chiel C. van Heerwaarden[1]

[1]Meteorology and Air Quality Group, Wageningen University & Research, Wageningen, the Netherlands

Key Points:

- We correct simulations of shallow cumulus cloud days with 1D radiative transfer for the 3D radiative effects in a post-processing step
- The probability distributions of diffuse and global radiation closely match the observations after filtering the surface diffuse radiation
- The filter size can be parameterized as a linear function of one or multiple cloud variables, resulting in a minimal computational overhead

Corresponding author: Mirjam Tijhuis, `mirjam.tijhuis@wur.nl`

Abstract

Most atmospheric models consider radiative transfer only in the vertical direction (1D), as 3D radiative transfer calculations are too costly. Thereby, horizontal transfer of radiation is omitted, resulting in incorrect surface radiation fields. The horizontal spreading of diffuse radiation results in darker cloud shadows, whereas it increases the surface radiation in clear sky patches (cloud enhancement). In this study, we developed a simple method to account for the horizontal transfer of diffuse radiation. We spatially filter the surface diffuse radiation field with a Gaussian filter, which is conceptually simple and computationally efficient. We applied the filtering to the results of Large-Eddy Simulations for two summer days in Cabauw, the Netherlands, on which shallow cumulus clouds formed during the day. We obtained the optimal filter size by matching the simulation results with detailed high-quality observations (1Hz). Without the filtering, cloud enhancements are not captured, and the probability distribution of global radiation is unimodal, whereas the observed distribution is bimodal. After filtering, the probability distribution of global radiation is bimodal and cloud enhancements are simulated, in line with the observations. We found that small changes in the filter width do not strongly influence the results. Furthermore, we showed that the width of the filter can be parameterized as a linear function of e.g. the cloud cover. Hence, this work presents a proof-of-concept for our method to come to more realistic surface irradiances by filtering diffuse radiation at the surface.

Plain Language Summary

The pattern of radiation at the surface is characterized by the presence of cloud shadows and peaks in the radiation caused by scattering of light by clouds. The amount of solar radiation that reaches the Earth's surface determines how much energy is produced by solar panels and how much heat and moisture is supplied to the clouds, thus it influences how the clouds develop. Existing models neglect the scattering of radiation in the horizontal direction, therefore the high peaks in the radiation are not modelled. In this paper, we show for two days with shallow cumulus clouds how we can include the effect of the horizontal propagation of radiation. We redistribute the radiation at the surface, and we compare our model results with measurements. After the redistribution, the high peaks in radiation are modeled. In general, we get a good match between the observed and modelled radiation distribution. We show that the redistribution can be made a function of the clouds in the model. Hence, this work presents a proof-of-concept for our method to come to more realistic surface radiation, without complex calculations.

1 Introduction

The amount of solar energy that reaches the earth surface is strongly influenced by the complex interactions between clouds and radiation. Therefore, solar energy partly reaches the surface directly and partly reaches the surface as diffuse radiation after it is scattered in the atmosphere by gases, aerosols and clouds. The total amount of solar energy reaching the surface, also referred to as surface irradiance or global radiation, governs many processes at the surface. It drives the sensible and latent heat fluxes, which supply moisture and energy to boundary layer clouds and thus determine their development. Apart from the surface fluxes, the surface irradiance also influences plant photosynthesis, as diffuse radiation is taken up by the canopy more efficiently than direct radiation (Kanniah et al., 2012). Furthermore, surface irradiance determines the production of renewable energy by solar panels. It is therefore important to have a good model representation of the surface irradiance and the partitioning between direct and diffuse radiation.

Currently, clouds as well as radiation are usually parameterized in weather and climate models. Existing parameterizations for radiation generally neglect the horizontal transport of radiation. Radiative transfer is considered in 1D and within separate vertical columns (Independent Column Approximation, ICA), to keep calculations affordable. Recent methods (Schäfer et al., 2016; Hogan et al., 2016) can account for the horizontal transport of radiation through cloud sides within grid boxes, making it possible to include the mean 3D effects in general circulation models. Between grid boxes, the horizontal transport can only be neglected if the grid boxes are large enough such that a cloud and its shadow fall within the same grid cell (Wapler & Mayer, 2008). As computing capacity increases, so does the model resolution. With that it becomes possible to resolve individual clouds in limited area models and horizontal transport of radiation between grid boxes is no longer negligible (Wissmeier et al., 2013). In Large-Eddy Simulations (LES), clouds and their full 3D structure are resolved explicitly, while the calculation of radiative transfer remains generally 1D. To make a next step in realism, it becomes increasingly relevant to improve existing parameterizations to account for the horizontal transport of radiation.

There are two major effects of the horizontal transport of radiation that cause the differences between radiative transfer in 1D and 3D. Firstly, in 1D, the cloud shadow is located exactly below the cloud. In reality, the cloud shadow is displaced and elongated. The displacement of the cloud shadow can impact the cloud size (Veerman et al., 2020), trigger secondary circulations (Gronemeier et al., 2017) and increase the formation of cloud streets (Jakub & Mayer, 2017). Secondly, the diffuse radiation reaches the surface exactly under the cloud in 1D. In reality, diffuse radiation is spread out over a larger surface area (Wissmeier et al., 2013; Wapler & Mayer, 2008; Hogan & Shonk, 2013). The horizontal spreading of the diffuse radiation results in more uniformly dark cloud shadows, whereas it increases the surface radiation in clear sky patches (cloud enhancement). Recently, Villefranque and Hogan (2021) provided the observational evidence for the 3D radiative effects. The horizontal spreading of radiation causes the characteristic bimodal distribution of solar irradiance observed under cloudy conditions (Schmidt et al., 2007, 2009; Gristey et al., 2020b; Kreuwel et al., 2020). Gristey et al. (2020b) showed that the probability distribution of global radiation of simulations with 1D radiative transfer clearly differs from the distribution of global radiation of observations and simulations with 3D radiative transfer. This difference is caused by the lack of horizontal spreading of diffuse radiation. Therefore, the spreading of the diffuse radiation is the focus point of this study.

Different methods exist to include 3D radiative effects or account for them. Radiative transfer can be computed accurately in 3D, for example with a Monte Carlo simulation (Mayer, 2009), but these calculations are orders of magnitude slower than 1D calculations. A more efficient 3D method is the TenStream solver (Jakub & Mayer, 2015). However, with the TenStream solver the surface fields of diffuse radiation are not diffused enough (Jakub & Mayer, 2015) and the calculations are still more than an order of magnitude slower than 1D calculations (Veerman et al., 2020; Jakub & Mayer, 2015). The probability distribution of the global radiation can also be predicted from cloud field properties with machine-learning (Gristey et al., 2020a). Alternatively, 1D radiative transfer calculations can be adapted to account for the 3D radiative effects. Such adaptations include the spatial information that is necessary to study the impact of the 3D effects on the simulations, which is not possible with the method of Gristey et al. (2020a). Furthermore, such adaptations are computationally more efficient than Monte Carlo simulations or the TenStream solver. Therefore, adaptations of 1D radiative transfer calculations can potentially be applied to longer time ranges and larger domains.

Existing literature shows that the errors in the location and shape of the cloud shadow can be tackled by using tilted columns (Tilted Independent Column Approximation, TICA) (e.g., Wissmeier et al., 2013; Wapler & Mayer, 2008; Várnai & Davies, 1999). The spreading of the diffuse radiation can be included by smoothing the 1D diffuse radiation fields (Nonlocal Independent Column Approximation, NICA, Marshak et al. (1995)). Especially these smoothing methods strongly simplify the actual radiative transfer. It is therefore very important to thoroughly validate the performance of these methods. In previous work, the smoothed 1D radiation was validated against 3D simulations for snapshots of cloud fields (Marshak et al., 1995; Zuidema & Evans, 1998; Wapler & Mayer, 2008; Wissmeier et al., 2013). Instead, we will use observations for the development and validation of our smoothing method, which allows us to test our method over a period of time. Different options exist to smooth the diffuse radiation. The simplest option is to use the area average diffuse radiation for the whole study area (Wapler & Mayer, 2008), which works well for small domains sizes with a regular cloud field, but often a more generally applicable approach, such as a smoothing filter, is required. Possible filters use a gamma distribution (Marshak et al., 1995) or a Gaussian distribution (Zuidema & Evans, 1998; Wissmeier et al., 2013). The simplest distribution, the Gaussian, requires the determination of only one parameter, the standard deviation (sigma). Sigma can be parameterized for use in operational models. Wissmeier et al. (2013) proposed a method where sigma is a function of the solar zenith angle and the distance from the center of the surface pixel to the center of the base of the closest cloud. This method requires the calculation of many sigmas, as sigma differs per surface pixel.

The aim of this study is to correct 1D radiative transfer calculations for the 3D radiative effects. We focus on the spreading of the shortwave diffuse radiation at the surface as this is essential to capture the cloud enhancements and more uniformly dark cloud shadows. We will use a spatial filter to smooth the diffuse radiation at the surface. We strive to keep the parameterization as simple as possible, thus we will use one filter size per time step for the whole domain and we will investigate the possibilities to describe this filter size as a linear function of one or a couple of cloud variables. As we aim to investigate the potential of the filtering, we will apply the filtering as a post-processing step to our LES output. We base our filtering on and validate our filtering against observations, as observations are available for long periods of time, for which 3D calculations are not feasible anymore. Additionally, the advantage of observations is that they are measurements of reality and not influenced by any model parameterization or assumption. We will study two shallow cumulus cloud days in Cabauw, the Netherlands, for which high-resolution observations (1Hz) are available from the Baseline Surface Radiation Network (BSRN) station.

2 Data

For this study, we selected two summer days (4 July and 15 August 2016) in Cabauw, the Netherlands, during which shallow cumulus clouds formed. The 3D radiative effects are most pronounced when cloud shadows and regions with cloud enhancements both occur frequently, thus we selected days with highly variable surface global radiation. Furthermore, ice and liquid water impact radiation differently, thus we selected days without high clouds (which contain ice). Lastly, we are interested in clouds that are surface driven, as the formation of these clouds is the result of the local surface irradiance. Therefore, we selected days that started and ended with cloud-free skies and had shallow cumulus clouds during the day.

We compared the simulation results (as described in the next section) with observations from the Royal Netherlands Meteorological Institute (KNMI) observatory in Cabauw. Cabauw is located in the centre of the Netherlands (51.971 °N, 4.927 °E), where the surroundings are flat and mainly consist of meadows and ditches. At the measurement site, basic meteorological variables such as specific humidity, temperature and wind speed are measured at 7 levels along a 200 m high tower (KNMI Data Services, 2022b). The cloud cover is measured with a NubiScope, which is a scanning infrared radiometer (KNMI Data Services, 2022a). These observations all have a 10 min resolution. We used these observations to validate the general performance of the LES model. For the main analyses, we used the observed shortwave irradiances (global, direct and diffuse) from the Baseline Surface Radiation Network (BSRN) site in Cabauw. At this station, broadband irradiances are measured at a single location with a high frequency (1 Hz). Details about the radiation measurements can be found in Knap (2018).

Apart from the observations, the clear sky radiation is available every minute, as calculated with the McClear model (Gschwind et al., 2019). The clear sky radiation is the amount of radiation that would have reached the surface if there were no clouds present.

3 Methods

3.1 Model Simulation

We performed realistic LESs using MicroHH (Van Heerwaarden et al., 2017). Our simulations use an interactive land-surface scheme, similar to HTESSEL (Balsamo et al., 2009) and our land surface is a homogeneous grassland. The 1D radiative transfer is calculated every 10 sec with RTE+RRTMGP (Pincus et al., 2019), using delta-scaling of the cloud optical properties. We simulate realistic weather conditions by coupling our LES to ERA5 with a method similar to the one described by e.g Neggers et al. (2012) and Schalkwijk et al. (2015). In short, in this setup, the atmosphere and soil are initialised from ERA5. Furthermore, the large scale forcings acting on the LES domain are reconstructed from ERA5 and added to the LES as time and height varying external forcings. These forcings are the advective tendencies of potential temperature, humidity and wind, the subsidence velocity, and geostrophic wind components. The domain mean state of the simulations is nudged towards ERA5 at a time scale of 3 hours, to prevent long experiments from drifting away from reality. For 4 July, the humidity close to the surface is much lower in ERA5 compared to the observations, thus we increased the initial humidity with 10% at the surface, and a linearly decreasing percentage above until roughly 1000 m (50 model levels). Additionally, we increased the nudging timescale to 12 h in the lowest 2 km (82 levels), to prevent the model from going towards the too dry ERA5 data.

Our domain has a size of 25.6 km x 25.6 km x 17 km, with a horizontal resolution of 50 m and a vertical grid spacing that increases with height, starting with 20 m grid spacing at the surface. Our LES uses double-periodic boundary conditions. We ran the simulations from 6 to 18 UTC (8-20 local time) and we saved the domain average statistics every 5 min. Additionally, we saved, every 10 sec, the results for an individual column in the centre of the domain (x = y = 12.8 km) and the horizontal cross sections for some key variables: liquid water path (including ice), shortwave downward radiation at the surface (both global and direct), cloud base height, cloud top height.

We investigated the probability distributions to compare the modeled radiation with the observations. We used the Probability Density Functions (PDFs) as used by Gristey et al. (2020b). These PDFs show the relative occurrence of the radiation values. Therefore, they provide insight into the occurrence and strength of cloud shadows and cloud enhancements. Apart from changes in the cloud field, PDFs based on time series include the effect of the changing solar zenith angle (SZA). We correct for the changing SZA by dividing the radiation values of both the simulation and the observations by cos(SZA) when PDFs are considered. Hereby, the radiation is normalised to a 0 degree solar zenith angle or, in other words, it is the radiation value as if the sun was right above the observer. For all PDFs, we used a binsize of 20 W m^{-2} and we resampled the observations to 10 sec averages, to match with the model resolution.

3.2 Smoothing Diffuse Radiation

We used a Gaussian filter to account for the 3D effects on diffuse radiation. This filter convolves the surface diffuse radiation from the 1D radiative transfer model with a Gaussian distribution. This means that the diffuse radiation at one point becomes a weighted average of the point itself and its neighbours. In 1D, the weights are described by a Gaussian distribution (G_{1D}) of the form:

$$G_{1D}(x) = \frac{1}{\sqrt{2\pi}\sigma_{\text{filter}}} \exp\left(\frac{-x^2}{2\sigma_{\text{filter}}^2}\right).$$

In which σ_{filter} is the standard deviation of the distribution and x is the distance from the point of interest. The filter includes the neighbours within four times the standard deviation (σ_{filter}), so x ranges between -4σ_{filter} and +4σ_{filter}. At the borders of the domain, the data is wrapped, meaning that data from the opposite side of the domain is included in the convolution. This is in line with the periodic boundaries of the simulations. To filter in 2D, 1D convolutions are performed in both horizontal directions subsequently. We tested the filtering for σ_{filter} between 0 and 1.5 km, in steps of 50 m, to determine the optimal sigma (σ_{opt}). We determine σ_{opt} per time step. as we apply the Gaussian filter per time step.

3.3 Determining the Optimal Filter Size

We determine σ_{opt} by comparing the simulation with the observations. The simplest way to do this is to compare the standard deviation of the observations with the standard deviation of the simulated field. From the simulation, we used the standard deviation of the diffuse radiation PDF after filtering ($\text{std}_{\text{smooth}}$). This means that $\text{std}_{\text{smooth}}$ is calculated over a smoothed field normalised by cos(SZA). Thus, $\text{std}_{\text{smooth}}$ is calculated per time step. The standard deviation of the observations (std_{obs}) is calculated from the time series between 10 and 16 UTC, normalised by cos(SZA) . Therefore, std_{obs} is constant. We consider the filtered distribution optimal if $\text{std}_{\text{smooth}}$ is as close as possible to std_{obs}. The impact of using the standard deviation as the optimization criterion is discussed in section 5, as well as the impact of using std_{obs} for all time steps.

3.4 Parameterization for the Filter Size

The optimal filter size (σ_{opt}) is a characteristic of the distribution of diffuse radiation, thus it is related to the cloud field. Therefore, σ_{filter} might be calculated as a function of properties of this cloud field. A possible parameterization was proposed by Wissmeier et al. (2013). Their parameterization involves the calculation of σ_{filter} per grid cell per time step. We investigated the possibilities to have a parameterization with less different values of σ_{filter} by using one σ_{filter} per time step for the whole domain. We tested parameterizations of the simple form: $\sigma_{\text{filter}} = cv$, in which c is a constant and v a variable related to the cloud field. In section 5, we will discuss further how well one filter size can be used for the entire domain.

From existing literature, it is expected that σ_{filter} is related to the cloud base height and/or the solar zenith angle (Wissmeier et al., 2013; Wapler & Mayer, 2008). On top of that, we hypothesize that σ_{filter} is related to the sizes of the individual clouds, as the effect of small clouds can be filtered away with a narrow filter, whereas the effect of large clouds needs a wider filter to be filtered out. We used the maximum cloud size as a measure for the cloud sizes present in the cloud field. The maximum cloud size is determined using a cloud tracking algorithm, as described by Heus and Seifert (2013). In short, all columns with a Liquid Water Path (LWP) larger than 0 g m^{-2} that are connected to each other are considered to form one cloud. The cloud size is then simply the square root of the area of the cloud. Apart from the maximum cloud size, we consider the cloud thickness and cloud cover for the parameterization of σ_{filter} as these variables are related to the maximum cloud size (Van Laar et al., 2019). In summary, we considered cloud thickness, cloud cover, cloud base height, solar zenith angle, and maximum cloud size to determine the best parameterization for σ_{filter}.

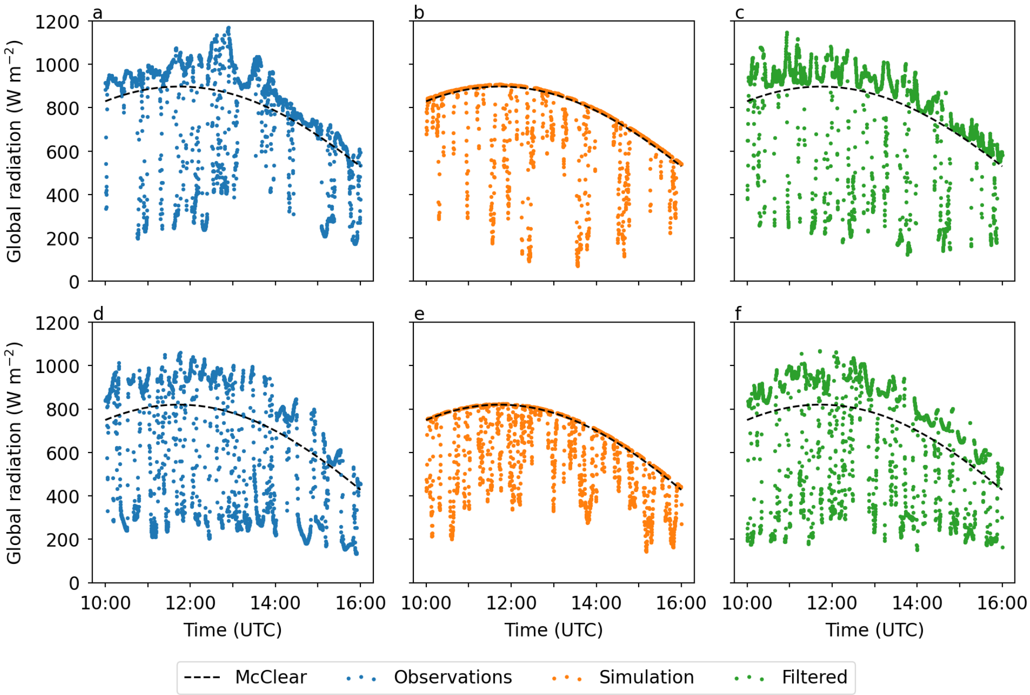

Figure 1. Timeseries of global radiation as (a) observed, (b) simulated and (c) filtered for 4 July. (d), (e) and (f) are as (a), (b) and (c), but for 15 August. For the simulations, the time series are taken at the centre point of the domain.

In addition to the single variable parameterizations, we investigate the improvement that can be obtained by using multiple linear regression. We start from the single variable parameterization that gives the best match (the highest correlation coefficient) with our σ_{opt}. We add one variable at a time and determine which combination gives the highest correlation with σ_{opt}.

4 Results

We will first show the general development of the simulations and compare it to the observations. Then, we will discuss the distribution of the radiation in detail, followed by the filtering of the radiation and the possible parameterizations for this filter.

4.1 Case Description and Model Validation

The timeseries of observed global radiation (Fig. 1a, d) show that the global radiation is either higher or lower than under clear sky conditions. The global radiation is lower than the clear sky value in a cloud shadow. When there is no cloud shadow, the radiation is enhanced by diffuse radiation scattered by a nearby cloud. In the simulation with 1D radiative transfer (Fig. 1b, e), the global radiation is either lower than or equal to the radiation under clear-sky conditions, meaning that cloud shadows occur, but cloud enhancements are not simulated. The rightmost panels in Fig. 1 show the timeseries after we filtered the diffuse radiation. These will be discussed in section 4.3.

Fig. 2 shows the timeseries of cloud cover, temperature and humidity. Comparing the model simulations with the observations shows that the simulations accurately cap-

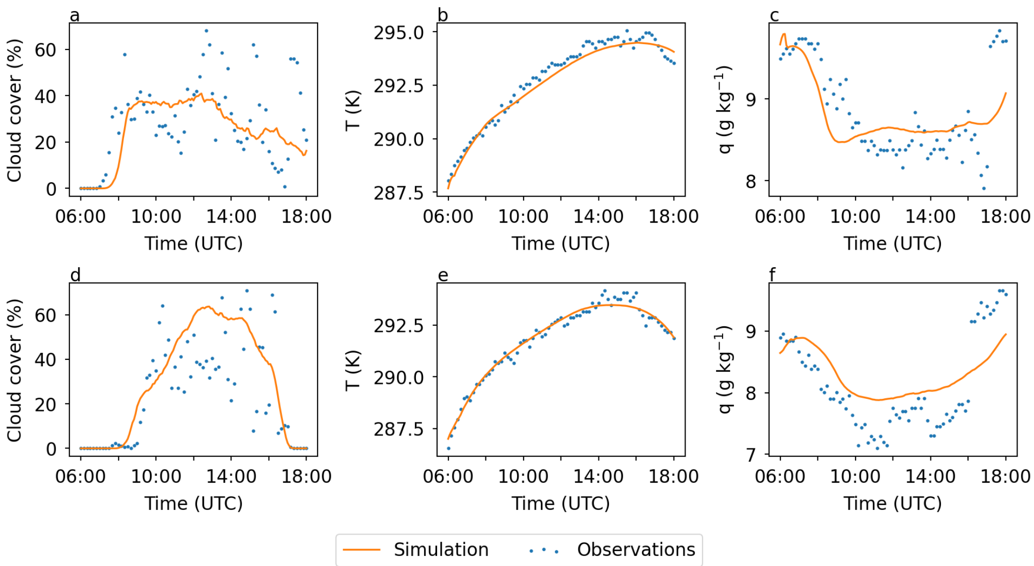

Figure 2. Time series of (a) cloud cover, (b) temperature and (c) specific humidity for 4 July. (d), (e) and (f) are as (a), (b) and (c), but for 15 August. Temperature and humidity are at 10m height.

ture realistic weather conditions. The simulation results are more smooth, because they are average values over the model domain, whereas the observations are at one location. For 4 July, the simulated cloud onset is about half an hour later than in the observations, whereas for 15 August it is about half an hour earlier. Although the modelled cloud structures will never be exactly as observed, the average cloud cover is well simulated for both days. Veerman et al. (2022) showed for the case of 15 August 2016 that a similar cloud cover is modelled when 3D radiative transfer calculations are used.

The simulated vertical profiles (Fig. 3) show that, in both cases, a stable boundary layer was present at the beginning of the day, at 6 UTC. The addition of sensible heat caused the boundary layer to grow and heat up. In the afternoon, the boundary layer was well mixed. On 4 July, the humidity above the boundary layer increases over time, but the changes are only small close to the boundary layer top. In general, only small changes in the profiles occur above the boundary layer, indicating that large scale advection plays a minor role. On both days, the local surface fluxes determine the development of the profiles during the day, which makes these days suitable case studies. The profiles of liquid water show that clouds are formed under the inversion (Fig. 3c, f). On the 15^{th} of August, a strong inversion (7 K) was present at the top of the boundary layer (Fig. 3d, e). The clouds spread out horizontally under the inversion, as the inversion prevents the clouds from growing in the vertical. This causes relatively thin clouds and a high cloud cover (Fig. 2d) for a case with shallow cumulus clouds. The clouds on both days clearly differ in their thickness and liquid water content. Thus, we can get an indication of how well our method works for shallow cumulus conditions, by testing our filtering method for these two days. In the remainder of this paper, we will focus on the hours between 10 UTC and 16 UTC when clouds are observed and simulated on both days.

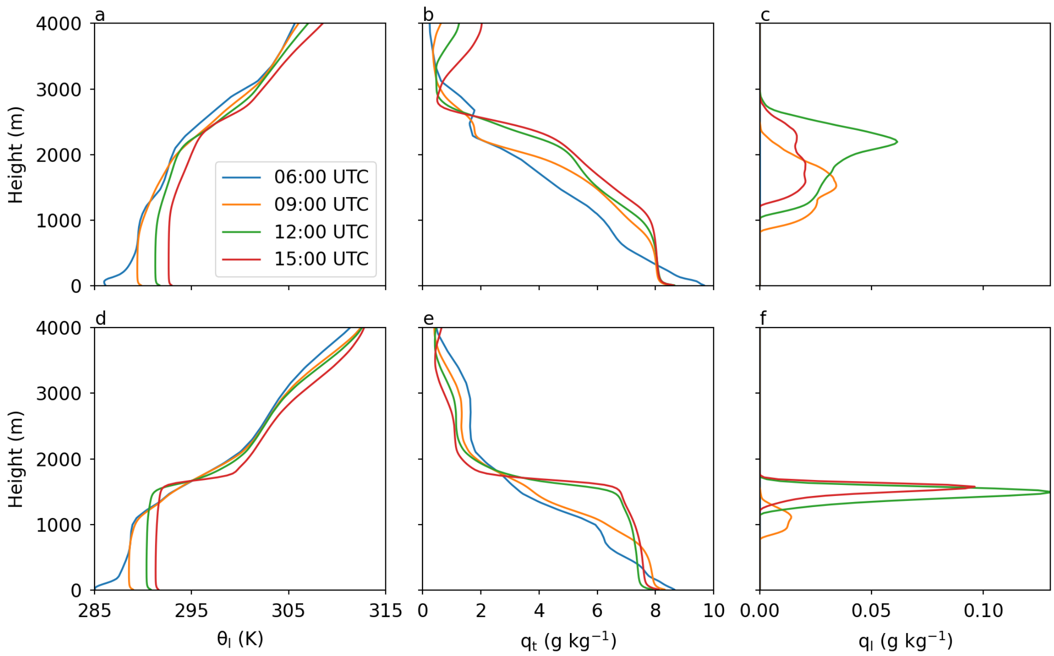

Figure 3. Domain-average vertical profiles of (a) liquid water potential temperature, (b) specific humidity, (c) liquid water specific humidity for 4 July. (d), (e) and (f) are as (a), (b) and (c), but for 15 August.

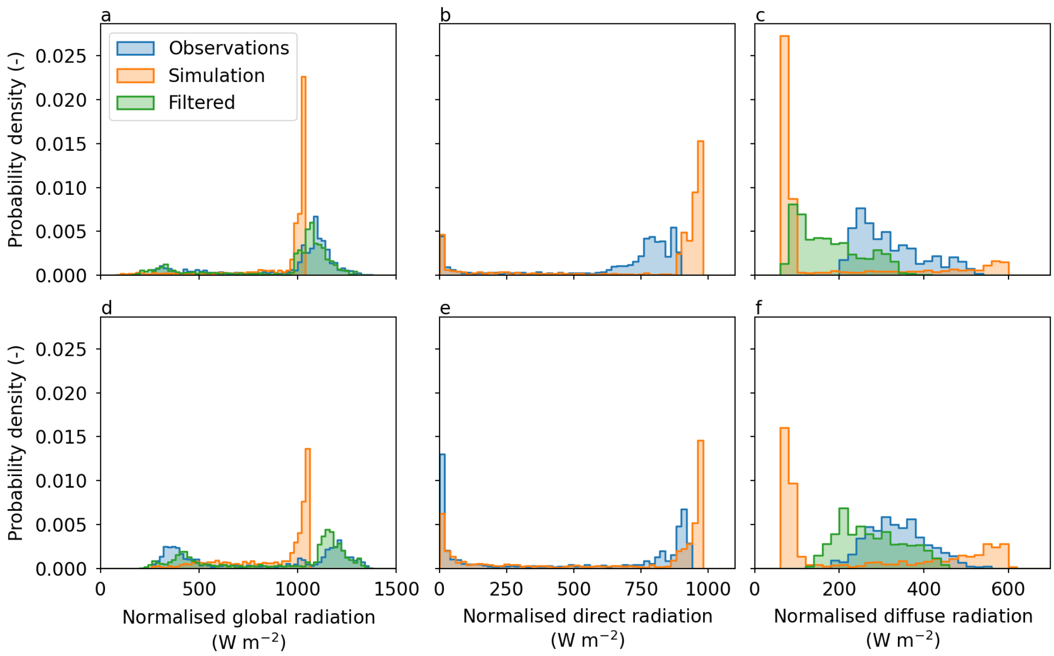

Figure 4. PDFs of (a) global radiation, (b) direct radiation, (c) diffuse radiation for the observations, the original simulation and the simulation after filtering for 4 July. (d), (e) and (f) are as (a), (b) and (c), but for 15 August. For these PDF, the time series from 10 to 16 UTC are used. For the simulation, the time series is taken at the centre point of the domain. All values are normalised by cos(SZA).

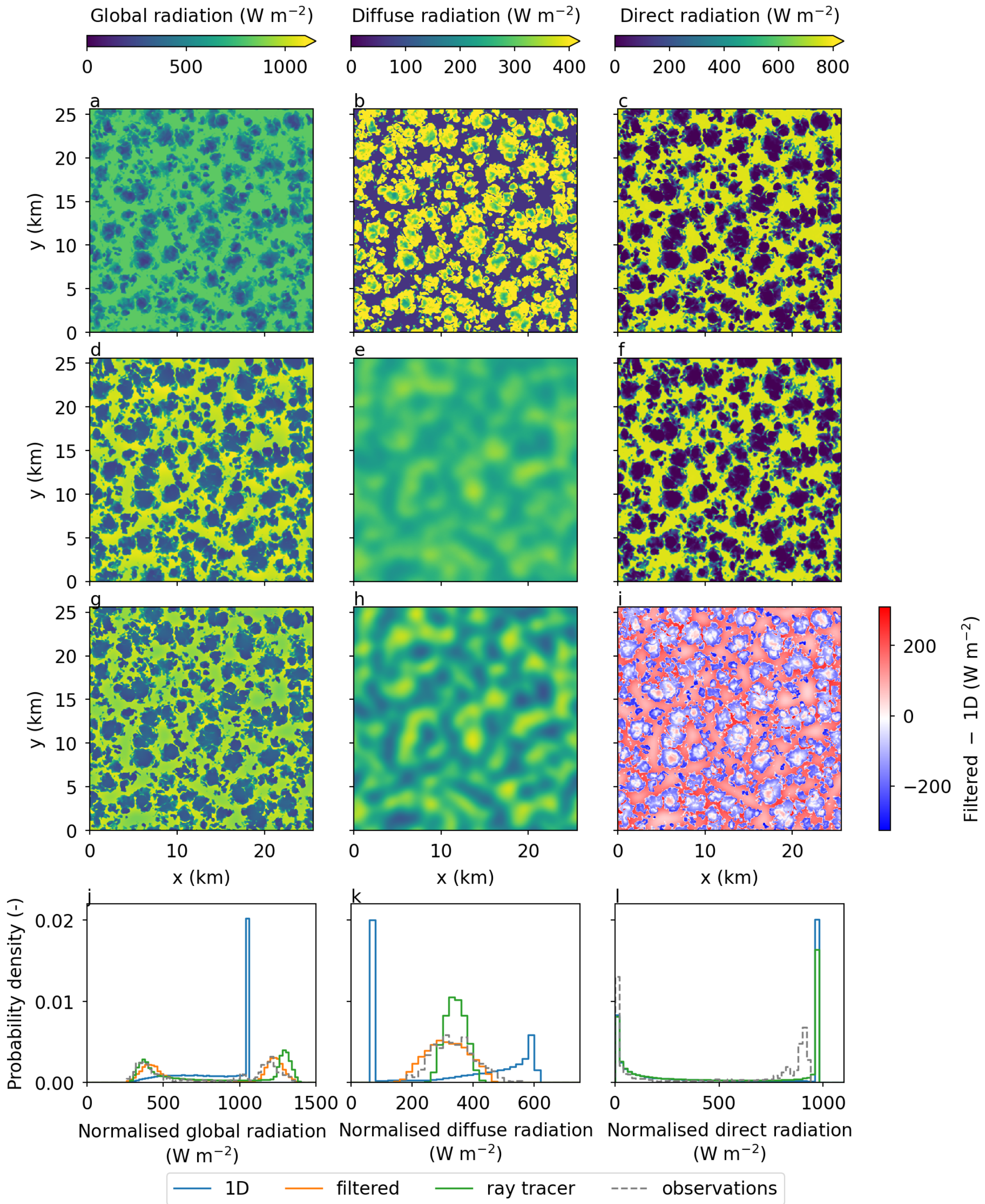

Figure 5. Surface fields at 15 August 12 UTC. The first row shows the original fields of (a) global radiation, (b) diffuse radiation, and (c) direct radiation. The second row shows the fields obtained with Monte Carlo ray tracing of (d) global radiation, (e) diffuse radiation and (f) direct radiation. The third row shows the fields after filtering the diffuse radiation of (g) global radiation and (h) diffuse radiation. (i) shows the difference in radiation between the original and filtered simulation. Note that we did not change the direct radiation. Therefore, the difference in (f) is the difference in diffuse radiation (b vs e) as well as the difference in global radiation (a vs d). The SZA is 37.9°. The fourth row shows the PDFs of (j) global radiation, (k) diffuse radiation, and (l) direct radiation corresponding to the fields in (a) until (h). For the PDFs of the observations, the time series between 10 and 16 UTC are used.

4.2 1D Radiative Transfer

In this section, we examine the surface irradiance from the simulation with 1D radiative transfer by looking at PDFs of global, direct and diffuse radiation (Fig. 4) and an example of the surface radiation fields in the simulation (Fig. 5, top row). We will first discuss the differences between the observations and the simulation with 1D radiative transfer. The PDFs and surface fields of the simulation after filtering will be discussed in the next section.

The simulated distribution of global radiation does not resemble the observed distribution (Fig. 4a, d). This is in line with the results of Gristey et al. (2020b) and Schmidt et al. (2007). The differences between the observations and the simulation can be explained by considering the direct and diffuse radiation separately (Fig. 4) and from the spatial patterns (Fig. 5, top row).

The direct radiation is close to zero in the cloud shadows and around 800 w m^{-2} in other areas (Fig. 5c). The simulated diffuse radiation is highest under the clouds (Fig. 5b). This partly compensates for the reduced direct radiation. Under the clouds, the diffuse radiation is highest, up to 500 W m^{-2}, in areas with a low LWP. In areas with a high LWP, the diffuse radiation is reduced as more radiation is absorbed and more radiation is scattered back upwards. In simulations with 1D radiative transfer, the cloud shadows are located exactly below the clouds (Fig. 5c). From simple geometry, it is clear that the shadow of a cloud is not directly below a cloud, unless the sun is right above the cloud. Additionally, the cloud shadows are too small in simulations with 1D radiative transfer, as only the top of the cloud intercepts radiation. In reality, the radiation falls on the cloud under an angle, thus part of the cloud sides also intercepts radiation, causing a larger cloud shadow. Previous studies showed that the, more complex, Tilted Independent Column Approximation (TICA) can be used to simulate the cloud shadows correctly in terms of both size and location (Wapler & Mayer, 2008; Várnai & Davies, 1999).

The spatial radiation patterns result in the PDFs shown in Fig. 4. The PDFs of the direct radiation show peaks around zero and between 800 and 1000 w m^{-2}, for both observations and simulations (Fig. 4b, e). The high values of simulated direct radiation are higher than the maximum observed direct radiation. On 4 July, the simulated values are up to 74 W m^{-2} more than the maximum observed, on 15 August up to 37 W m^{-2}. In line with this overestimation, the average diffuse radiation is underestimated (Fig. 4c, f). This is also observed for the clear sky radiation, indicating that the difference might be the effect of aerosols, which are not included in the radiation calculations. The impact hereof is discussed in section 5. The simulated diffuse radiation PDF is dominated by amounts of diffuse radiation around 50 W ,$^{-2}$, that occur under clear sky conditions. This diffuse radiation is the result of scattering by gases. The large peak in the PDF is clearly not in line with the observed PDF (Fig. 4c, f). Thus, for the days and times shown in fig. 4, we find that the differences in the smoothness of the global radiation field and thereby the shape of the global radiation PDF are primarily caused by differences in the diffuse radiation, which is in line with the findings of Gristey et al. (2020b). Hence, we will focus on accounting for the horizontal transport of diffuse radiation to get the PDF correct.

4.3 Smoothing Diffuse Radiation

We applied a spatial filter, to account for the horizontal spreading of diffuse radiation. Then, we combined the filtered diffuse radiation with the original direct radiation, to obtain the new global radiation. This means that we introduced the horizontal spreading of the diffuse radiation, but not the 3D effect on the direct radiation. Fig. 5g, h shows an example of the resulting surface radiation fields. The difference between the original and filtered fields is shown in Fig. 5i. The difference in Fig. 5i is the difference in diffuse radiation as well as the difference in global radiation, as we did not change the direct radiation. The difference plot makes clear how the filtering influences the radiation. Diffuse radiation is reduced in the regions where it was originally the highest, thus under the clouds. Diffuse radiation is increased in the regions where it was originally low, thus in the clear sky patches and in the centres of the clouds. In the example cross sections of diffuse radiation at the surface in Fig. 5b, h, diffuse radiation under the clouds is reduced with a maximum reduction of 327 W m^{-2} and in clear sky patches it is increased with a maximum of 310 W m^{-2}. The cross section in Fig. 5h shows that the highest amounts of diffuse radiation still occur below the clouds, but the areas around the clouds also receive diffuse radiation. This is in line with the results of Wissmeier et al. (2013), who showed that filtering the diffuse radiation can greatly improve the surface radiation fields. Combining the filtered diffuse radiation field (Fig. 5e) with the original direct radiation field (Fig. 5c) results in the global radiation field shown in Fig. 5d. This global radiation field shows cloud enhancements in addition to the cloud shadows and clear sky patches.

For comparison, we performed a 3D radiative transfer calculation for this time step. To this end, we took the cloud field from our simulation with 1D radiative transfer and performed Monte Carlo ray tracing, as described in Veerman et al. (2022) but with delta-scaled cloud optical properties. The surface irradiance fields obtained with the ray tracing are shown in Fig. 5d, e, f. Fig. 5 j, k and l show the PDFs corresponding to the fields in Fig. 5a until h. In the direct radiation fields, we see that with 3D radiative transfer, the cloud shadows are shifted northwards compared to the 1D simulation. The diffuse radiation field is much more smooth with 3D radiative transfer compared to 1D radiative transfer. The ray tracer, as well as the filtered 1D simulation, shows a single peak in the diffuse radiation PDF, in contrast with the two peaks of the 1D simulation. Also compared to our filtered diffuse radiation field, the 3D radiative transfer calculations give a more smooth diffuse radiation field. This results in a narrower distribution for the ray tracer compared to the filtered 1D simulation. As a result of the more smooth diffuse field, the cloud enhancements are larger in the 3D simulation, compared to our filtered simulation. This is visible both in the surface fields and in the PDFs. In Fig. 5 j, k and l, the distribution of the observations is also shown. The simulated distributions should be compared with the observations with care, as the observations are at one location over 6 hours, and the simulations are a field at one time. It is clear that by filtering the 1D simulations, a close match with the observations is obtained in this time step. This in line with our expectations, as our filter size is chosen such that we match the observations as good as possible.

The impact of the filtering is also clearly visible in the timeseries (Fig. 1c, f) and corresponding PDFs (Fig. 4). The shape of the simulated diffuse radiation PDFs closely matches the shape of the observed PDF, when the diffuse radiation is filtered with the optimal filter width (σ_{opt}). The PDFs of global radiation are now bimodal. There is one peak below 500 W m^{-2}, showing that the cloud shadows became more uniformly dark. The second peak is at higher irradiance values than the original peak, showing that the irradiance in regions other than the cloud shadows is increased. The bimodal PDFs of global radiation can also be obtained directly from the characteristics of the cloud field by using machine learning as shown byGristey et al. (2020a). By filtering the diffuse radiation, we provide not only the global radiation statistics, but also the partitioning between direct and diffuse radiation, as well as an indication of how the radiation is distributed spatially. This spatial information is essential to couple a parameterization for the 3D radiative effects to an LES in the future.

The cloud enhancements are also clearly visible in the timeseries (Fig. 1c, f). Before filtering, the McClear value was simulated in the clear sky periods. After filtering, the cloud enhancements are simulated and their magnitude is in line with the peaks in the observations. Furthermore, before filtering, some cloud shadows were much darker than others. After filtering, the cloud shadows are more similar, which is also in line with

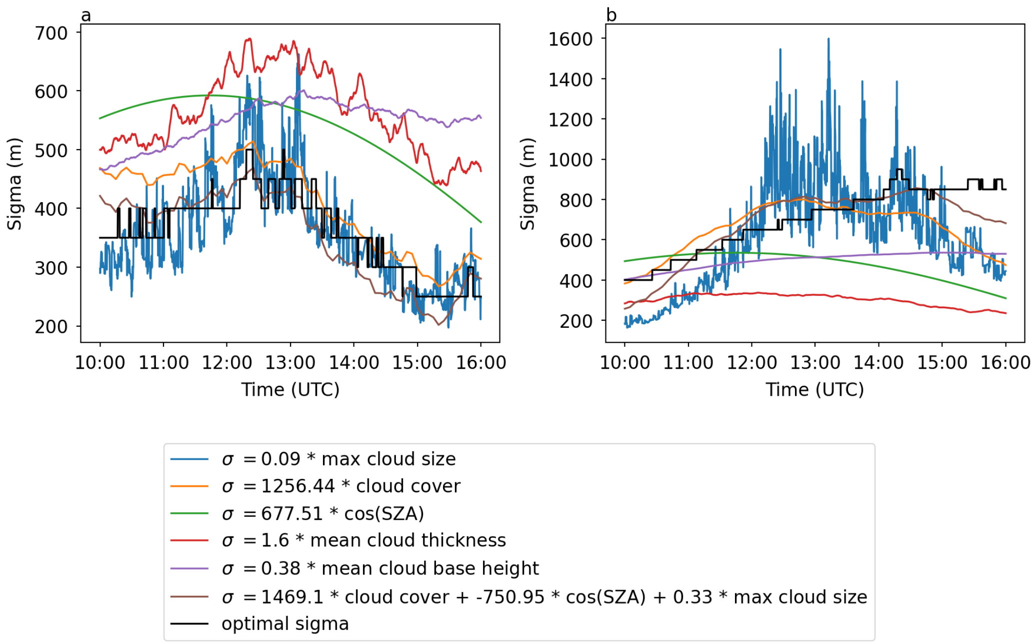

Figure 6. Time series of σ_{filter} for (a) 4 July and (b) 15 August (b). σ_{opt} and σ_{filter} as a linear function of the individual cloud variables, as well as the combination of cloud cover, cos(SZA) and mean cloud base height.

the observations. Together, Fig. 4 and Fig. 1 show that our filtering method greatly improves the model results.

4.4 Sigma Parameterization

Next, we want to parameterize σ_{filter} as a function of the cloud properties in the simulation, to be able to filter the diffuse radiation in a simulation. Therefore, we investigated how well σ_{opt} can be described as a function of cloud thickness, cloud cover, cloud base height, solar zenith angle, and maximum cloud size. The time series of σ_{opt} are shown in Fig. 6. Note that for 15 August, the range of σ shown is larger than for 4 July. On the 15$^{\text{th}}$ of August, σ_{opt} increases during most of the period and is fairly constant at the end. On the 4$^{\text{th}}$ of July, σ_{opt} increases a bit in the first three hours and decreases afterwards. The average σ_{opt} on 15 August is 700 m, which is close to the 625 m found by Wissmeier et al. (2013) for their case with cumulus mediocris. For 4 July, we find a smaller average σ_{opt} of 360 m.

The optimal filter size (σ_{opt}) can be parameterized by relating it to the cloud field. Fig. 6 shows simple approximations of σ_{opt}. Regarding the trends, the maximum cloud size, cloud cover, cos(SZA) and mean cloud thickness all show an increase in the beginning of the period and a decrease later on. For 4 July, this is exactly what we also observe for σ_{opt}. For 15 August, we do not find a decrease in σ_{opt} at the end of the period, which is best captured by the approximation based on the cloud base height. Regarding the values, we find that using cos(SZA), mean cloud thickness or mean cloud base height gives an overestimation of the filter size on 4 July and an underestimation of the filter size on 15 August. The estimates based on the maximum cloud size and cloud cover capture the trends more closely. However, especially near the end of the period on 15 August, the estimates based on cloud cover and maximum cloud size also underestimate

Table 1. Correlation coefficient (r) showing the correlation between σ_{opt} and possible parameterizations of σ_{filter} using different (combinations of) variables.

variable(s)	r
cloud cover	0.830
cos(SZA)	-0.473
maximum cloud size	0.728
mean cloud thickness	-0.736
mean cloud base	-0.113
cloud cover, cos(SZA)	0.874
cloud cover, maximum cloud size	0.833
cloud cover, mean cloud thickness	0.854
cloud cover, mean cloud base	0.829
cloud cover, cos(SZA), maximum cloud size	0.874
cloud cover, cos(SZA), mean cloud thickness	0.884
cloud cover, cos(SZA), mean cloud base	0.937
cloud cover, cos(SZA), mean cloud base, maximum cloud size	0.941
cloud cover, cos(SZA), mean cloud base, mean cloud thickness	0.943
cloud cover, cos(SZA), mean cloud base, mean cloud thickness, maximum cloud size	0.944

the optimal filter size by up to a factor two. The advantage of the cloud cover is that it is readily available in the model, whereas the maximum cloud size has to be obtained with a cloud tracking algorithm (Heus & Seifert, 2013), and hence induces additional computational cost.

Table 1 shows the correlation coefficients between σ_{opt} and approximations based on different variables. First, the correlation coefficients for the single variable approximations are shown. The highest correlation is obtained when we use the cloud cover. We also performed multiple linear regressions. As we obtained the highest correlation with a single variable when using the cloud cover, we did multiple linear regression with two variables: the cloud cover and one of maximum cloud size, cos(SZA), mean cloud thickness and mean cloud base height. The correlation increases most when cos(SZA) is added. We continued adding variables to the combination with the highest correlation coefficient until a multi linear regression with all variables. Adding the cos(SZA) and mean cloud base height increased the correlation from 0.83 to 0.94. Adding than also the mean cloud thickness and maximum cloud size resulted in an increase in correlation of less than 0.01.

To fully capture the development of σ_{opt} more complex methods, such as machine learning, can potentially be used. For example, Gristey et al. (2020a) used machine learning to directly predict the PDFs of global radiation from a set of cloud field properties.

During the two days that we studied, especially the cloud cover and maximum cloud size are clearly correlated with each other ($r > 0.8$). It is possible that this correlation, which is undesired if both variables are used in a multiple linear regression, is specific to the chosen shallow cumulus cases. To carefully check whether the parameters included are independent of each other, a larger dataset is required. In addition, given the limited size of our dataset, there is also a chance that a multiple linear regression overfits when using too many variables. We will therefore continue by using the simple approximations of the filter size based on cloud cover only and cloud cover, cos(SZA), and mean cloud base height. Hereby, we can investigate how sensitive the resulting diffuse radiation PDF is to the used filter size.

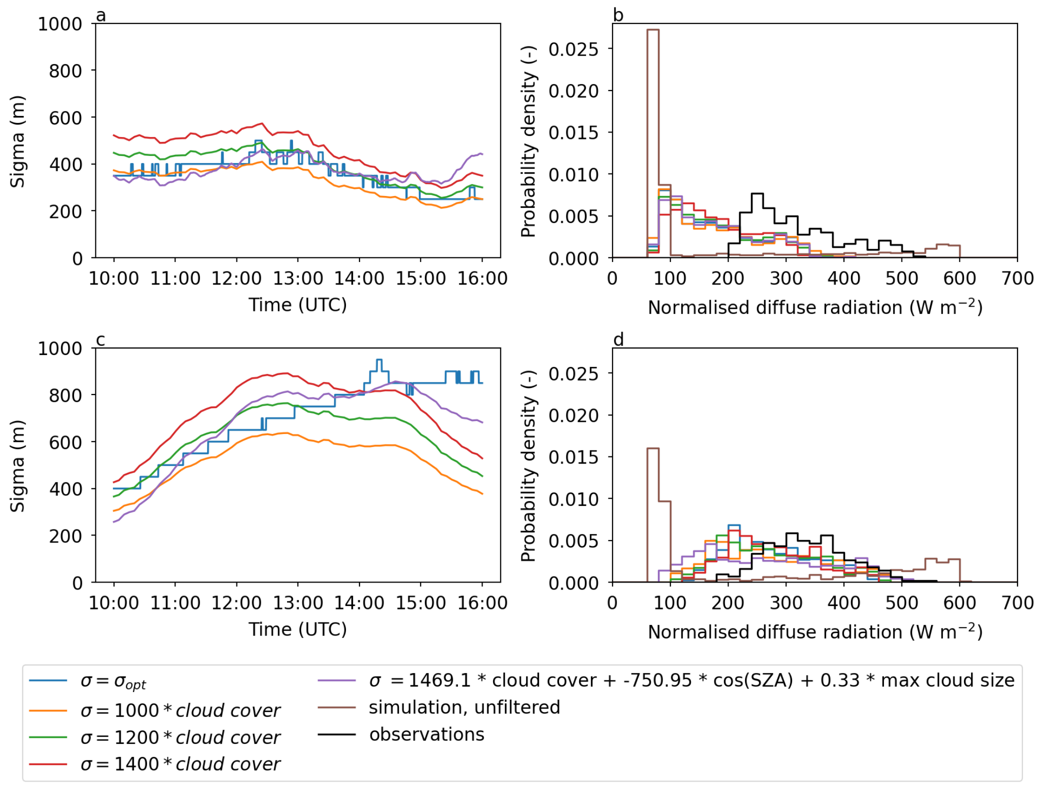

Figure 7. (a) timeseries of σ_{opt} and approximations of σ_{filter} as a function of the cloud cover. (b) PDFs of the diffuse radiation for the observations, original 1D simulation and filtered simulation. For these PDF, the time series from 10 to 16 UTC are used. For the simulation, the time series is taken at the centre point of the domain. All values are normalised by cos(SZA). For the filtering, the σ's from (a) are used. (c) and (d) are as (a) and (b), but for 15 August.

4.5 Sigma Sensitivity

It is important to know how sensitive the resulting PDFs are to a change in σ_{filter}, as σ_{filter} differs depending on which parameterization is used. We defined three possible approximations of σ_{opt} as a function of the cloud cover, with the constant being 1000, 1200 and 1400 (Fig. 7a, c). For most of the times, all three approximations are close to σ_{opt}. Only for the last part of 15 August, the parameterizations deviate strongly from σ_{opt}. In addition, 7 a, c shows σ_{filter} based on the cloud cover, cos(SZA) and mean cloud base height. Fig. 7b and d show the PDFs of diffuse radiation that are obtained when using the different approximations of σ_{filter}. The differences between the three possible approximations based only on the cloud cover are small, as well as the differences between the approximations based only on cloud cover, the approximation based on three variables and σ_{opt}. By eye, it is not possible to tell which one of these PDFs matches the PDFs of the observations best. This shows that with a rough approximation of σ_{filter} we can reach a clear improvement, compared to the original 1D radiative transfer calculations.

5 Discussion

In this section, we reflect on the assumptions made while comparing the observations to the simulations.

First, we assumed that one value for $\mathrm{std}_{\mathrm{obs}}$ is representative for the hours between 10 and 16 UTC. Calculating $\mathrm{std}_{\mathrm{obs}}$ over different, shorter periods results in different values for $\mathrm{std}_{\mathrm{obs}}$, which would have resulted in different values for σ_{opt}. Ideally, the timespan over which $\mathrm{std}_{\mathrm{obs}}$ is calculated is related to the changes in the cloud field. If the cloud field changes, the standard deviation should change accordingly. However, the averaging period should also be long enough to have a statistically reasonable estimate for $\mathrm{std}_{\mathrm{obs}}$. Furthermore, $\mathrm{std}_{\mathrm{obs}}$ depends on the clouds that pass over the sensor and the size of these clouds in the direction of the wind. A better representation of the cloud field in all directions can be obtained by performing measurements in a grid. Gristey et al. (2020b) used observations from 10 locations to study the relation between the cloud fraction and the cloud radiative effect. Their results indicate that the observation density should be at least one order of magnitude larger to be able to detect the relationships found in model simulations. Alternatively, one could base σ_{opt} on a 3D simulation instead of observations, as was done before by e.g. Wissmeier et al. (2013) and Zuidema and Evans (1998).

Second, we assumed that σ_{filter} is optimal if the resulting standard deviation of the diffuse radiation field is as close as possible to the standard deviation of the observed diffuse radiation. A matching standard deviation does not guarantee that the PDFs also have a similar shape. To determine the impact hereof, we determined σ_{opt} also from the shapes of the PDFs of diffuse radiation. To this end, we described the shape of the observed PDF by fitting a gamma distribution through it. Then, we determined σ_{opt} by minimizing the Euclidean distance between the filtered PDF and the fitted gamma-distribution. There was no clear improvement in the PDFS, although the obtained σ_{opt} based on the shape is in general a bit larger. We therefore argue that the simple matching of the standard deviations functions well enough.

Third, a matching standard deviation also does not guarantee that the PDFs have a similar mean. From Fig. 4c, f, it became clear that the diffuse radiation is on average too low in our simulations. This underestimation has three possible causes. The modelled and observed clouds might be slightly different. Although the cloud cover is similar in the observations and simulations, the cloud structures might be different. Furthermore, clouds and radiation interact differently in 1D compared to reality. In reality, a fraction of the photons leaves the clouds on the sides after only a few scattering events. Therefore, statistically, these photons are likely to be scattered forward, thus towards the surface. In 1D calculations, these photons do not leave the clouds, so they are likely scattered again. As these photons are scattered multiple times, the chances increase that these photons are scattered back upwards, reducing the amount of diffuse radiation that reaches the surface. However, we also find an underestimation of the clear-sky diffuse radiation, which cannot be related to differences in the cloud field. This underestimation is likely caused by the absense of aerosols in the radiation computations. The underestimation is larger on 4 July (maximum 70 W m^{-2}) than on 15 August (maximum 50 W m^{-2}), which is in line with the larger aerosol optical depth on 4 July compared to 15 August. (We compared the aerosol optical depths from the McClear model (Gschwind et al., 2019), not shown.) For broken cloud conditions, Schmidt et al. (2009) and Gristey et al. (2022) showed that aerosols reduce the irradiance in the gaps between the clouds, by scattering radiation to the cloudy regions. In 1D simulations, the radiation scattered by aerosols cannot propagate horizontally to the cloudy regions, thus it will reach the surface in the gaps between the clouds. Thus in our PDFs, the diffuse radiation in the gaps between the clouds will increase. How the PDF will change exactly depends on the properties of the aerosols. As the optical depth of the aerosols is much smaller than the optical depth of the cumulus clouds, there will still be a large difference in diffuse radiation between the cloudy regions and the gaps between the clouds. Therefore, we argue that filtering the diffuse radiation can still be used to mimic the effect of the horizontal propagation of diffuse radiation. As the initial distribution of diffuse radiation is different when aerosols are included, the optimal filter size will also be different. This means that the possible parameterizations in Fig. 6 and Fig. 7 are designed for very clean conditions and have to be updated when aerosols are included. Aerosols do not only scatter radiation (direct effect of aerosols), but aerosols also interact with nearby clouds (indirect effect of aerosols). The relative importance of these effects is uncertain as it depends on characteristics of both the clouds and the aerosols (Boucher et al., 2013).

Fourth, we assumed that one σ_{filter} can be used for the whole domain. On the two selected days, the cloud properties were homogeneous in space over an area larger than our domain size. For these cases, our results show that we can greatly improve the radiation field with one filter size. With that we show that σ_{filter} can be related to the statistical properties of the cloud field. Thus, the filter size does not have to vary on the scale of a single cloud, which is the case in Wissmeier et al. (2013), where they use the distance from the center of the surface pixel to the center of the base of the closest cloud. Instead, the filter size can varies on the scales on which the statistical properties of the cloud fields vary. This does mean that when the domain is larger and/or the cloud properties are not statistically the same in the whole domain, more than one σ_{filter} will be required.

6 Conclusion

In this work, we described a simple approach to correct the unrealistic surface solar irradiance fields that arise from LES with 1D radiative transfer. Horizontal transfer of radiation is omitted in 1D, resulting in a misplacement of the cloud shadows and a lack of horizontal spreading of diffuse radiation. We approximated the horizontal spreading of the diffuse radiation by filtering the diffuse radiation at the surface with a Gaussian filter. We determined the optimal width of the Gaussian filter by comparing our simulations to observations. We applied this approach to two case studies with shallow cumulus clouds. For these cases, filtering the diffuse radiation resulted in a PDF of global radiation that closely matches the observations. The time series of global radiation after filtering show the characteristic cloud enhancements that were not simulated with the 1D radiative transfer model. The width of our filter can be approximated with a linear function of only one cloud variable. For the two shallow cumulus cloud cases that we analyzed, we found that the best approximation of the filter width with one variables is $\sigma_{\text{filter}} \approx 1250\ \textit{cloud cover}$. Changing the fitting constant to 1000 or 1400, or adding additional variables does not result in a visually worse result.

The results show that the used approach has the potential to correct for the 3D radiative effect by adding minimal changes to existing methods. This assures that the impact on computational times is small. First tests showed that the filtering increases the total runtime of the model with less than 1%. Therefore, this method has the potential to be applied to many more days and different locations in the future.

Our results suggest that our method could be further improved by including aerosols, especially on days with a high aerosol optical depth, as this should reduce the overestimation of direct radiation and accompanying underestimation of diffuse radiation. In addition, the filtering of the diffuse radiation can be combined with the tilted column approach, that can correct the direct radiation for the 3D radiative effects. Furthermore, one can consider extending the filtering to the longwave spectral range.

Extending to many more days will allow for further generalization to different cloud regimes and will give more insight in the usability of a single variable parameterization and the added value of a multiple variable parameterization. A larger dataset will allow to split the dataset in a training and test dataset, which would give insight in the robustness of our parameterization.

In short, we have shown that filtering the surface diffuse radiation has the potential to give more realistic surface irradiances with minimal additional computational cost. We applied the filtering as a post-processing step, which directly improves model results regarding the surface, for example when studying the impact of radiation on renewable energy production by solar panels or the impact on surface processes such as photosynthesis. Additionally, coupling the filter to the LES can potentially contribute to a better representation of the surface fluxes and with that a better representation of the cloud dynamics.

7 Open Research

The observations of temperature, humidity and cloudcover at the measurement station in Cabauw are openly available from the KNMI Data Platform (`https://dataplatform.knmi.nl/dataset/cesar-tower-meteo-lc1-t10-v1-0` and `https://dataplatform.knmi.nl/dataset/cesar-nubiscope-cldcov-la1-t10-v1-0`, last accessed 16 September 2022). The observations of radiation are available in Knap and Mol (2022) and Mol et al. (2022). The model simulations are performed with MicroHH (Van Heerwaarden et al., 2017) and the used version is available at `https://github.com/microhh/microhh/tree/develop`. All other data and scripts used to conduct this research are added for peer review in the folder data&scripts.zip. This information will be made available in a repository once the manuscript is accepted.

Acknowledgments
We acknowledge funding from the Wageningen Institute for Environment and Climate Research (WIMEK) and the Shedding Light On Cloud Shadows project funded by the Dutch Research Council (NWO) (grant: VI.Vidi.192.068). B.v.S. acknowledges funding from the Ruisdael Observatory, co-financed by the Dutch Research Council (NWO) under grant number 184.034.015. The simulations are carried out on the Dutch national e-infrastructure with the support of SURF Cooperative.

References

Balsamo, G., Beljaars, A., Scipal, K., Viterbo, P., van den Hurk, B., Hirschi, M., & Betts, A. K. (2009). A revised hydrology for the ECMWF model: Verification from field site to terrestrial water storage and impact in the Integrated Forecast System. *Journal of hydrometeorology*, *10*(3), 623–643.

Boucher, O., Randall, D., Artaxo, P., Bretherton, C., Feingold, G., Forster, P., ... Zhang, X. (2013). Clouds and aerosols. In *Climate change 2013: the physical science basis. Contribution of Working Group I to the Fifth Assessment Report of the Intergovernmental Panel on Climate Change* (pp. 571–657). Cambridge University Press.

Gristey, J., Feingold, G., Glenn, I., Schmidt, K., & Chen, H. (2020b). Surface solar irradiance in continental shallow cumulus fields: Observations and large-eddy simulation. *Journal of the Atmospheric Sciences*, *77*(3), 1065–1080.

Gristey, J., Feingold, G., Glenn, I. B., Schmidt, K. S., & Chen, H. (2020a). On the relationship between shallow cumulus cloud field properties and surface solar irradiance. *Geophysical Research Letters*, *47*(22), e2020GL090152.

Gristey, J., Feingold, G., Schmidt, K. S., & Chen, H. (2022). Influence of aerosol embedded in shallow cumulus cloud fields on the surface solar irradiance. *Journal of Geophysical Research: Atmospheres*, *127*(11), e2022JD036822.

Gronemeier, T., Kanani-Sühring, F., & Raasch, S. (2017). Do shallow cumulus clouds have the potential to trigger secondary circulations via shading? *Boundary-Layer Meteorology*, *162*(1), 143–169.

Gschwind, B., Wald, L., Blanc, P., Lefèvre, M., Schroedter-Homscheidt, M., & Arola, A. (2019). Improving the McClear model estimating the downwelling solar radiation at ground level in cloud-free conditions – McClear-v3. *Meteorologische Zeitschrift*, *28*(2), 147-163.

Heus, T., & Seifert, A. (2013). Automated tracking of shallow cumulus clouds in large domain, long duration large eddy simulations. *Geoscientific Model Development*, *6*(4), 1261.

Hogan, R., Schäfer, S. A., Klinger, C., Chiu, J. C., & Mayer, B. (2016). Representing 3-D cloud radiation effects in two-stream schemes: 2. Matrix formulation and broadband evaluation. *Journal of Geophysical Research: Atmospheres*, *121*(14), 8583–8599.

Hogan, R., & Shonk, J. (2013). Incorporating the effects of 3D radiative transfer in the presence of clouds into two-stream multilayer radiation schemes. *Journal of the atmospheric sciences*, *70*(2), 708–724.

Jakub, F., & Mayer, B. (2015). A three-dimensional parallel radiative transfer model for atmospheric heating rates for use in cloud resolving models—The TenStream solver. *Journal of Quantitative Spectroscopy and Radiative Transfer*, *163*, 63–71.

Jakub, F., & Mayer, B. (2017). The role of 1-D and 3-D radiative heating in the organization of shallow cumulus convection and the formation of cloud streets. *Atmospheric Chemistry and Physics*(21), 13317–13327.

Kanniah, K., Beringer, J., North, P., & Hutley, L. (2012). Control of atmospheric particles on diffuse radiation and terrestrial plant productivity: A review. *Progress in Physical Geography*, *36*(2), 209–237.

Knap, W. (2018). *Basic and other measurements of radiation at station Cabauw (2018-08)* [data set]. PANGAEA. Retrieved from `https://doi.org/10.1594/PANGAEA.893843` doi: 10.1594/PANGAEA.893843

Knap, W., & Mol, W. B. (2022). *High resolution solar irradiance variability climatology dataset part 1: direct, diffuse, and global irradiance.* Zenodo. Retrieved from `https://doi.org/10.5281/zenodo.7093164` doi: 10.5281/zenodo.7093164

KNMI Data Services. (2022a). *Clouds - cloud cover retrieved from infrared measurements at 10 minute intervals at cesar observatory.* Retrieved 2012-09-16, from `https://dataplatform.knmi.nl/dataset/cesar-nubiscope-cldcov-la1-t10-v1-0`

KNMI Data Services. (2022b). *Meteo profiles - validated and gapfilled tower profiles of wind, dew point, temperature and visibility at 10 minute interval at cabauw.* Retrieved 2012-09-16, from `https://dataplatform.knmi.nl/dataset/cesar-tower-meteo-lc1-t10-v1-0`

Kreuwel, F., Knap, W., Visser, L., van Sark, W., Vilà-Guerau de Arellano, J., & van Heerwaarden, C. (2020). Analysis of high frequency photovoltaic solar energy fluctuations. *Solar Energy*, *206*, 381–389.

Marshak, A., Davis, A., Wiscombe, W., & Cahalan, R. (1995). Radiative smoothing in fractal clouds. *Journal of Geophysical Research: Atmospheres*, *100*(D12), 26247–26261.

Mayer, B. (2009). Radiative transfer in the cloudy atmosphere. In *Epj web of conferences* (Vol. 1, pp. 75–99).

Mol, W. B., Knap, W. H., & van Heerwaarden, C. C. (2022). *High resolution solar irradiance variability climatology dataset part 2: classifications, supplementary data, and statistics.* Zenodo. Retrieved from `https://doi.org/10.5281/zenodo.7092058` doi: 10.5281/zenodo.7092058

Neggers, R. A., Siebesma, A., & Heus, T. (2012). Continuous single-column model evaluation at a permanent meteorological supersite. *Bulletin of the American*

Meteorological Society, *93*(9), 1389–1400.
Pincus, R., Mlawer, E., & Delamere, J. (2019). Balancing accuracy, efficiency, and flexibility in radiation calculations for dynamical models. *Journal of advances in modeling earth systems*, *11*(10), 3074–3089.
Schäfer, S. A., Hogan, R. J., Klinger, C., Chiu, J. C., & Mayer, B. (2016). Representing 3-D cloud radiation effects in two-stream schemes: 1. Longwave considerations and effective cloud edge length. *Journal of Geophysical Research: Atmospheres*, *121*(14), 8567–8582.
Schalkwijk, J., Jonker, H. J., Siebesma, A. P., & Bosveld, F. C. (2015). A year-long large-eddy simulation of the weather over cabauw: An overview. *Monthly Weather Review*, *143*(3), 828–844.
Schmidt, K., Feingold, G., Pilewskie, P., Jiang, H., Coddington, O., & Wendisch, M. (2009). Irradiance in polluted cumulus fields: Measured and modeled cloud-aerosol effects. *Geophysical research letters*, *36*(7).
Schmidt, K., Venema, V., Giuseppe, F. D., Scheirer, R., Wendisch, M., & Pilewskie, P. (2007). Reproducing cloud microphysical and irradiance measurements using three 3D cloud generators. *Quarterly Journal of the Royal Meteorological Society: A journal of the atmospheric sciences, applied meteorology and physical oceanography*, *133*(624), 765–780.
Van Heerwaarden, C., van Stratum, B., Heus, T., Gibbs, J., Fedorovich, E., & Mellado, J. (2017). MicroHH 1.0: a computational fluid dynamics code for direct numerical simulation and large-eddy simulation of atmospheric boundary layer flows. *Geoscientific Model Development*, *10*, 3145–3165.
Van Laar, T., Schemann, V., & Neggers, R. (2019). Investigating the diurnal evolution of the cloud size distribution of continental cumulus convection using multiday les. *Journal of the Atmospheric Sciences*, *76*(3), 729–747.
Várnai, T., & Davies, R. (1999). Effects of cloud heterogeneities on shortwave radiation: Comparison of cloud-top variability and internal heterogeneity. *Journal of the atmospheric sciences*, *56*(24), 4206–4224.
Veerman, M., Pedruzo-Bagazgoitia, X., Jakub, F., Vilà-Guerau de Arellano, J., & van Heerwaarden, C. (2020). Three-dimensional radiative effects by shallow cumulus clouds on dynamic heterogeneities over a vegetated surface. *Journal of Advances in Modeling Earth Systems*, *12*(7).
Veerman, M., van Stratum, B. J., & van Heerwaarden, C. C. (2022). Cumulus convection over land in cloud-resolving simulations with a coupled ray tracer. *arXiv preprint arXiv:2208.05247*.
Villefranque, N., & Hogan, R. J. (2021). Evidence for the 3d radiative effects of boundary-layer clouds from observations of direct and diffuse surface solar fluxes. *Geophysical Research Letters*, *48*(14), e2021GL093369.
Wapler, K., & Mayer, B. (2008). A fast three-dimensional approximation for the calculation of surface irradiance in large-eddy simulation models. *Journal of Applied Meteorology and Climatology*, *47*(12), 3061–3071.
Wissmeier, U., Buras, R., & Mayer, B. (2013). paNTICA: A fast 3D radiative transfer scheme to calculate surface solar irradiance for NWP and LES models. *Journal of applied meteorology and climatology*, *52*(8), 1698–1715.
Zuidema, P., & Evans, K. (1998). On the validity of the independent pixel approximation for boundary layer clouds observed during ASTEX. *Journal of Geophysical Research: Atmospheres*, *103*(D6), 6059–6074.